Inorganic Chemistry

Article

pubs.acs.org/IC

Impact of d-Orbital Occupation on Metal−Carbon Bond Functionalization

E. Chauncey Garrett, III, Travis M. Figg, and Thomas R. Cundari*

Center for Catalytic Hydrocarbon Functionalization, Department of Chemistry, and Center for Advanced Scientific Computing and Modeling (CASCaM), University of North Texas, 1155 Union Circle, #305070, Denton, Texas 76203-5017, United States

Supporting Information

ABSTRACT: Metal−carbon bond functionalization leading to C−O bond formation is a promising component reaction that can ultimately form the basis for production of methanol from natural gas. Two primary pathways have been considered: (1) an organometallic Baeyer−Villiger (OMBV) pathway, and (2) a two-step, redox oxy-insertion. A series of first-row transition metal−methyl complexes was modeled for these two pathways to elucidate any trend therein. Several important conclusions can be derived from this research. First, the OMBV mechanism for oxy-insertion is only preferred over the redox pathway in those cases when the metal−methyl's d^n electron count is such that the latter mechanism would render a chemically infeasible formal oxidation state for an oxo-methyl intermediate. Second, moving toward the so-called oxo wall effectively ameliorates one thermodynamic "sink" (i.e., oxo-Me intermediate) in the redox pathway. However, both oxy-insertion mechanisms suffer from the same feature that would thwart catalysis; i.e., the $[M^{II}]$−methoxide product is in a thermodynamic sink relative to the $[M^{II}]$−methyl reactant. Third, future experiments in hydrocarbon partial oxidation catalysis should focus on effecting oxy-insertion with the weakest oxidants and in establishing the linkage between thermodynamic and kinetic oxygen-atom transfer potentials of oxidants.

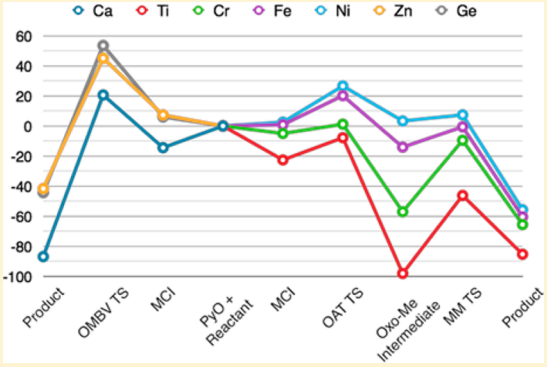

INTRODUCTION

Methanol is a highly desirable industrial product. Ideally, one would wish to convert methane to methanol in a single step using molecular oxygen as an oxidant at temperatures of <200 °C in order to minimize capital expenditures for a facility to perform this catalysis. Methanol can be used as a transportation fuel (it has a higher octane rating and faster flame speed in comparison to gasoline),[1] for wastewater denitrification,[1−3] to make DME (dimethyl ether, both a diesel substitute and a precursor to gasoline),[1] for biodiesel transesterification,[1] and as a fuel cell hydrogen carrier (methanol has more hydrogen atoms per gallon than any other liquid that is stable under ambient conditions).[1] Despite intense interest, a viable methane-to-methanol (MTM) catalyst remains elusive. Identification of catalysts for methane partial oxidation to methanol is a reaction for which computational chemistry can play an important role in elucidating key factors such as metal identity and metal d-orbital occupation leading to improved MTM catalysts.[1,4]

There are two primary steps in a catalytic cycle to make methanol: (1) C−O bond formation and (2) C−H activation. Our motivation for focusing on C−O bond formation as opposed to C−H activation lies in the relative paucity of literature precedents for the former transformation.[5−11] Carbon−hydrogen bond activation is extremely well studied; for example, Shilov and Shul'pin's classic review[12] has been cited over 1800 times! Our approach to identify the chemical factors that control selective methane oxidation is 2-fold: (1) elucidate trends as a function of metal identity in terms of preference for certain reaction pathways[13] and (2) discover promising systems for C−O bond formation (oxy-insertion) within a catalytic cycle that can ultimately form the basis for production of methanol from natural gas.

The literature on oxy-insertion has been discussed at length in previous publications by our group.[14,15] The most salient observation from these studies of metal-mediated C−O bond formation is that there are two main nonradical, reaction pathways: (1) an organometallic Baeyer−Villiger (OMBV) pathway, i.e., one-step, nonredox insertion of an oxygen atom into an M−C bond, and (2) a two-step, redox reaction in which an initial oxygen atom transfer (OAT) occurs to form an oxo intermediate (formally raising the metal oxidation state by 2 units) is followed by a methyl-migration (MM) to the oxo ligand to yield methoxide product. The latter is hereafter referred to as the OAT/MM mechanism. The precursor to oxy-insertion is formed by coordination of the oxidant (YO, pyridine-N-oxide in the present research) to the metal−methyl reactant complex and is denoted as the metallo-Criegee intermediate (MCI), $L_nMMe(YO)$, analogous to the Criegee intermediate in the organic BV reaction.[14,16]

Received: June 26, 2014
Published: July 10, 2014

   dx.doi.org/10.1021/ic5015048 | Inorg. Chem. 2014, 53, 7789−7798

A series of first-row transition metal methyl complexes was modeled. One of the motivations for their selection is the relationship between the relative Earth-abundance of said metals and therefore their low cost and environmental "greenness." Using standard criteria, all 3d transition metals are green with the exception of scandium.[17] One may argue that construction of a catalytic cycle for methane oxidation in which oxy-insertion occurs via an OMBV pathway opens up considerable flexibility for using Earth-abundant 3d transition metals given the lack of a formal redox step. The two-step OAT/MM process implies a metal with stable formal oxidation states separated by two units, which 3d metals do not typically possess. Additionally, in terms of atom economy, a single-step OMBV mechanism is preferred and potentially easier to control/design than a two-step OAT/MM mechanism.

As noted above, there are few experimental examples in which OMBV occurs and of those that do, to our knowledge, all occur in d^0 systems.[18−20] An important question is thus raised: are transition metal complexes other than those with a d-count of zero capable of effecting oxy-insertion via an OMBV pathway? In essence, the ultimate issue to be addressed in this paper is how does the metal's d-orbital occupation dictate the preferred oxy-insertion pathway?

COMPUTATIONAL METHODS

The Gaussian '09 software package[21] is utilized to model ground and transition states. Geometry optimizations and vibrational frequency calculations were obtained with density functional theory (DFT). The hybrid functional, combining Becke's three-parameter exchange functional, along with Lee, Yang, and Parr's correlation functional (B3LYP)[22−25] was employed in conjunction with the CEP-31G(d) basis set.[26] This standard level of theory has been used previously in studies of oxy-insertion.[14]

Transition states were distinguished from minima by the presence of a single imaginary frequency, obtained from the calculated energy Hessians. Though other (higher energy) pathways may have been identified, what is presented in this paper focuses on the lowest energy pathways calculated for each metal.

All plausible spin states were modeled for each metal system. Minimum energy crossing point (MECP) calculations were performed for systems in which a spin "flip" was thought to be significant using a code developed by Harvey and co-workers.[27−29] The calculated MECP energies and geometries implied that spin crossovers are expected to have limited impact on oxy-insertion for 3d metals.

Energetics are reported as free energies in kcal/mol and are computed at standard temperature and pressure (298.15 K and 1 atm). Starting structures were obtained from the Cambridge Structural Database (CSD).[30]

RESULTS AND DISCUSSION

The so-called oxo wall, delineated more than 50 years ago by Ballhausen and Gray,[31−33] is germane to the present research in that it may be postulated that complexes with d-orbital occupation numbers that do not support a stable metal-oxo bond will prefer oxy-insertion via a nonredox (i.e., OMBV) pathway. To test this hypothesis, a series of complexes were modeled that utilize the following metals, which in their reactant state, [M]−Me ([M] = metal-β-diketiminate model ligand), possess an even d-count: calcium (d^0), titanium (d^2), chromium (d^4), iron (d^6), nickel (d^8), zinc (d^{10}) and germanium (s^2d^{10} or "d^{12}") in order to elucidate any trend contained therein. The β-diketiminate supporting ligand was chosen for the present study because examples of low-coordinate (3−4 most commonly) alkyl complexes are known for these metals with β-diketiminate supporting ligation.[34−41] Note that for this research the oxidant is pyridine-N-oxide (PyO), which thus defines the leaving group as pyridine.

The set of metal centers modeled here is designed to delineate which factors (in particular, d-orbital occupation) influence the preferred oxy-insertion pathway. Each [M]−Me reactant was modeled for both proposed catalytic pathways, affording the possibility of either an OMBV or OAT/MM mechanism. It will be shown that calcium-, zinc-, and germanium-methyl complexes are calculated to prefer oxy-insertion via a single-step, nonredox (OMBV) pathway. All other metals calculated herein display a preference for the two-step, redox (OAT/MM) pathway for oxy-insertion.

Calcium. All calcium stationary points are singlets, as expected for a d^0 metal ion. Calcium was calculated to operate through an OMBV pathway. No oxo pathway was found; searches for an OAT/MM pathway for the singlet calcium complexes always collapse back to OMBV stationary points, as expected for a metal already in its highest stable oxidation state.

The coordination of the PyO oxidant to the trigonal planar calcium-methyl reactant complex, ^{1}[Ca]Me, is exergonic by −14.5 kcal/mol to form the metallo-Criegee intermediate (MCI), ^{1}[Ca](OPy)(Me), Figure 1. Inspection of the CSD[30]

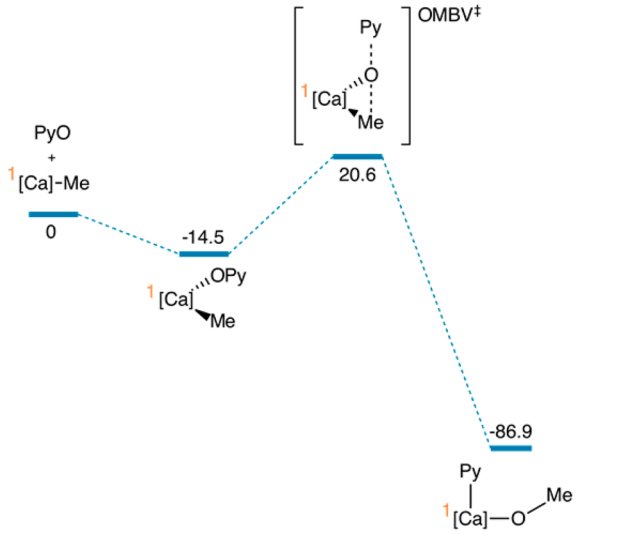

Figure 1. B3LYP/CEP-31G computed reaction coordinate (OMBV) for calcium−methyl complex. [Ca] = Ca-β-diketiminate model (see Figure 2). Numerical values are computed free energies in kcal/mol. The superscript prefix denotes the computed lowest energy multiplicity for that stationary point.

reveals that the Ca^{2+} ion typically is 6- or 8-coordinate. Thus, addition of PyO allows the calcium ion in ^{1}[Ca](OPy)(Me) to be four-coordinate, and thus marginally closer to a more typical coordination number for the Ca^{II} ion.

As calcium complexes are atypical choices for catalyst modeling studies, inspection of the calculated geometries was undertaken. From the CSD, mean Ca−C bond lengths are 2.65 Å with a sample standard deviation of 0.13 Å for n = 152 samples. In our system, the calculated Ca−C bond lengths are 2.54 Å (^{1}[Ca]Me reactant), 2.59 Å (^{1}MCI), and 2.59 Å (^{1}OMBV‡), Figure 2, all in reasonable accord with the crystallographic examples. The product Ca−O bond length is 2.01 Å. From the CSD, the mean Ca−O bond length (for alkoxide O ligands) is 2.29(13) Å (n = 26). Note that the majority of the experimental examples are six- or eight-coordinate about

dx.doi.org/10.1021/ic5015048 | Inorg. Chem. 2014, 53, 7789−7798

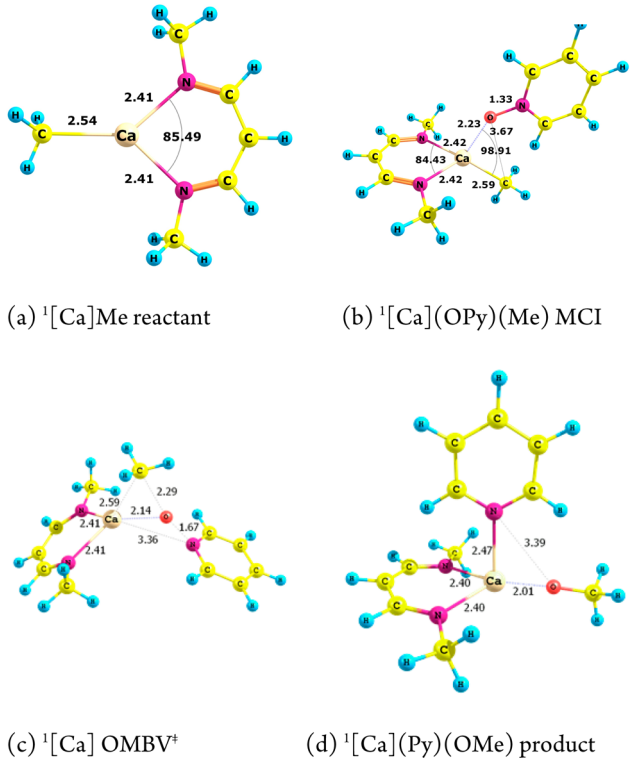

(a) ^{1}[Ca]Me reactant (b) ^{1}[Ca](OPy)(Me) MCI

(c) ^{1}[Ca] OMBV‡ (d) ^{1}[Ca](Py)(OMe) product

Figure 2. Selected B3LYP/CEP-31G(d) optimized geometries of calcium complexes calculated for the OMBV pathway. Bond lengths in Å. The superscript prefix denotes the computed lowest energy multiplicity for that stationary point.

calcium, and so one would expect the calculated value for trigonal planar ^{1}[Ca](Py)(OMe) to be closer to the low end of the experimental range.

From the pseudotetrahedral metallo-Criegee intermediate, Figure 2b, to the Baeyer–Villiger transition state, Figure 2c, is calculated to be uphill by 35.1 kcal/mol and hence ΔG_{rel} (free energy relative to separated PyO and methyl complex) = 20.6 kcal/mol, Figure 1. As with previously modeled OMBV transition states,[15,42,43] the displacement in the imaginary frequency of the transition state corresponds to the inserted oxygen atom "ping-ponging" between the methyl carbon that is to be oxy-inserted and the N of the pyridine leaving group, ν_i = 578i cm^{-1}. Likewise, the C–O–N angle is obtuse and the MCON active site of the calcium OMBV‡ is near planar, Figure 2c. Insertion of the oxygen atom into the Ca–C bond is highly exergonic, as expected for a highly electropositive metal, the products being ΔG_{rel} = −86.9 kcal/mol, Figure 1. Given a free energy barrier of ca. 30 kcal/mol, calcium organometallics would seem to be intriguing candidates for oxy-insertion experiments, although the thermodynamic "sink" that is ^{1}[Ca](Py)(OMe) obviously limits its potential for incorporation into full catalytic cycles.

The Ca–O bond may be used as a gauge of the OMBV transition state's "lateness" according to the Hammond Postulate since the bond is maintained throughout the calculated reaction coordinate, unlike the Ca–Me and Ca–N_{Py} bonds. The computed Ca–O bond lengths are 2.23 Å (MCI), 2.14 Å (OMBV‡), and 2.01 Å (product), Figure 2. Thus, the overall decrease in bond length from the metallo-Criegee intermediate to the product is δr_{M-O} = 0.22 Å. The calcium OMBV‡ is thus calculated to be "early" based on a bond length ratio of ca. 41% (0.09 Å/0.22 Å).

Zinc. All modeled zinc complexes are singlets. Like the calcium-methyl complex just discussed, the zinc variant was calculated to oxy-insert via an OMBV pathway. OAT/MM pathway searches for the singlet zinc complexes always collapse back to OMBV stationary points. As with calcium, this is expected for a metal already in its highest stable oxidation state. The coordination of the PyO oxidant to the trigonal planar ^{1}[Zn]Me reactant[34,44] is endergonic by 7.3 kcal/mol to form the MCI, ^{1}[Zn](OPy)(Me), Figure 3. In the Zn MCI complex,

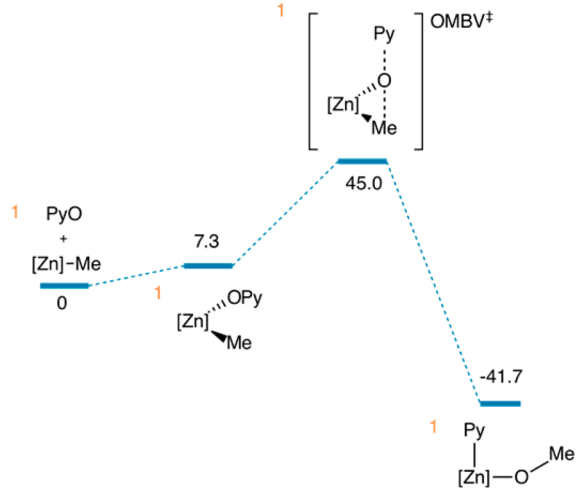

Figure 3. B3LYP/CEP-31G computed reaction coordinate (OMBV) for zinc-methyl complex. [Zn] = Zn-β-diketiminate model (see Figure 4). Numerical values are computed free energies in kcal/mol. The superscript prefix denotes the computed lowest energy multiplicity for that stationary point.

PyO is calculated to bind in the outer coordination sphere of the ^{1}[Zn]Me complex, Zn–O = 4.79 Å, Figure 4b, which is consistent with the computation that ^{1}[Zn](OPy)(Me) is uphill versus separated reactant and oxidant on the free energy surface, Figure 3. These results for the Zn metallo-Criegee intermediate are thus different from calcium. We propose that the difference is due to Zn^{2+} being a considerably smaller ion than Ca^{2+}, suggesting that the β-diketiminate ligand may more easily enforce a lower coordination number at the former metal: six-coordinate ionic radii, r_{ion} = 88 pm (Zn^{2+}), 114 pm (Ca^{2+}), 87 pm (Ge^{2+}), and 74 ppm (four-coordinate Zn^{2+} ion).[45]

From the trigonal planar MCI to the Baeyer–Villiger transition state (ν_i = 499i cm^{-1}), is calculated to be uphill by 37.7 kcal/mol (ΔG_{rel} = 45.0 kcal/mol) for the oxy-insertion transition state, Figure 3. Insertion of the oxygen atom into the Zn–C bond is highly exergonic, ΔG_{rel} = −41.2 kcal/mol.

The Zn–O bond is a tenuous gauge of the OMBV transition state's "lateness," given that the PyO oxidant lies in the outer coordination sphere of ^{1}[Zn]Me in the MCI. In the MCI, Zn–O = 4.79 Å; for the zinc OMBV‡, Zn–O = 1.90 Å; in the ^{1}[Zn](Py)(OMe) product, Zn–O = 1.88 Å, Figure 4. Thus, there is only a 0.02 Å difference between the Zn–O bond length in the OMBV‡ and the ensuing product. In comparison to the calcium complex, δr_{M-O} = 0.13 Å between the OMBV‡ and its methoxide product. The computed data thus imply a "later" TS for oxy-insertion by the zinc complex as compared to the calcium model.

Germanium. The coordination of the PyO oxidant to ^{1}[Ge]Me is endergonic by 6.0 kcal/mol to form the MCI,

dx.doi.org/10.1021/ic5015048 | Inorg. Chem. 2014, 53, 7789–7798

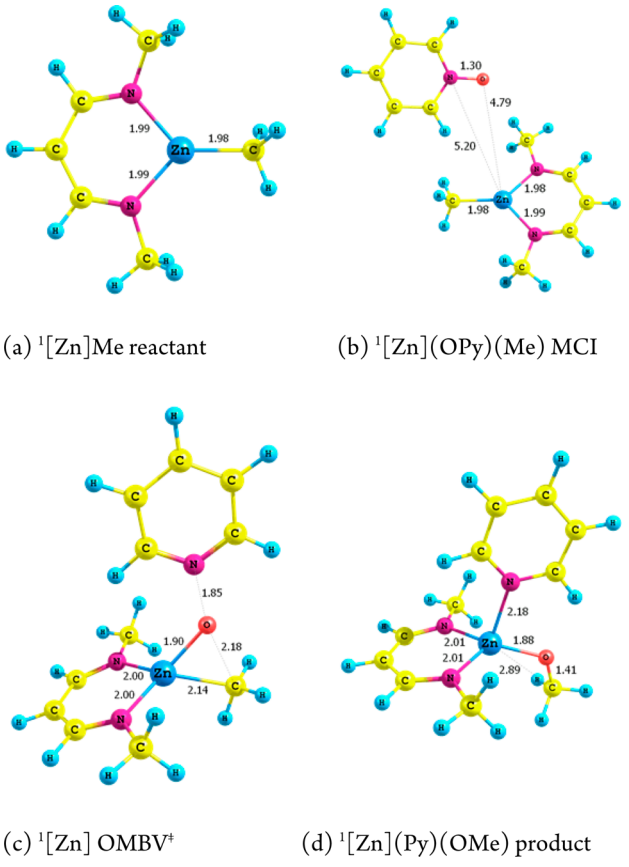

(a) ^{1}[Zn]Me reactant (b) ^{1}[Zn](OPy)(Me) MCI

(c) ^{1}[Zn] OMBV‡ (d) ^{1}[Zn](Py)(OMe) product

Figure 4. Selected B3LYP/CEP-31G(d) optimized geometries of zinc complexes calculated for the OMBV pathway. Bond lengths in Å. The superscript prefix denotes the computed lowest energy multiplicity for that stationary point.

^{1}[Ge](OPy)(Me). As with the zinc system just discussed, the oxidant is calculated to lie outside the inner coordination sphere of the metal for the germanium metallo-Criegee intermediate. From the singlet MCI to the singlet OMBV‡ is calculated to be uphill by 47.5 kcal/mol (ΔG_{rel} = 53.5 kcal/mol), Figure 5. Insertion of the oxygen atom into the Ge−ßC bond is highly exergonic as with all other metals thus far discussed, ΔG_{rel} = −44.3 kcal/mol. Interestingly, the exergonicity of oxy-insertion for the p-block germanium model is more similar to that computed for d-block zinc (ΔG_{rel} = −41.2 kcal/mol, Figure 3) than the s-block metal calcium (ΔG_{rel} = −86.9 kcal/mol, Figure 1).

Inspection of the calculated geometries was undertaken. From the CSD,[30] mean Ge−C bond lengths are 1.950(38) Å (n = 1110). For [Ge]−Me complexes, two examples were found in the CSD, with germanium−methyl bond lengths of 2.014 Å[35] and 2.002 Å.[36] In the present models, the calculated Ge−Me bond lengths are 2.04 Å (reactant), 2.03 Å (MCI), and 2.22 Å (OMBV‡), the former two being in reasonable accord with the crystallographic examples, while the latter indicates ca. 10% lengthening compared to the ground state minima ^{1}[Ge]Me and ^{1}[Ge](OPy)(Me), Figure 6. The product Ge−O bond length is 1.83 Å in ^{1}[Ge](OMe); from the CSD, the mean Ge−O bond length (three-coordinate Ge, alkoxide O ligands, and β-diketiminate supporting ligands) is 1.84(2) Å for a very small number of examples (n = 5).

As with other metals, the Ge−O bond was used as a gauge of the OMBV‡'s "lateness" via a Hammond Postulate analysis.

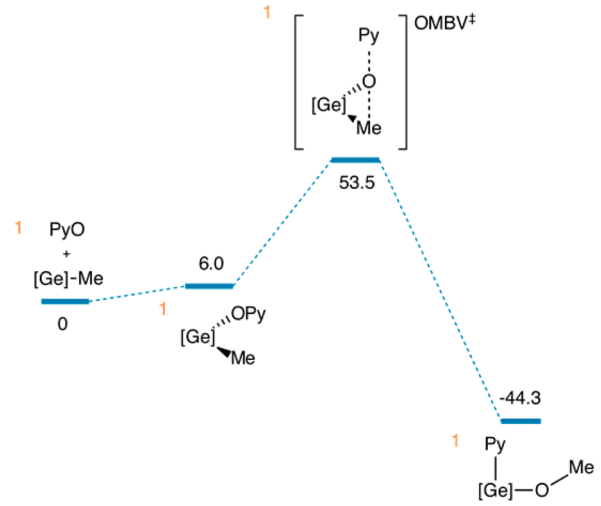

Figure 5. B3LYP/CEP-31G computed reaction coordinate (OMBV) for germanium−methyl complex. [Ge] = Ge-β-diketiminate model (see Figure 6). Numerical values are computed free energies in kcal/mol. The superscript prefix denotes the computed lowest energy multiplicity for that stationary point.

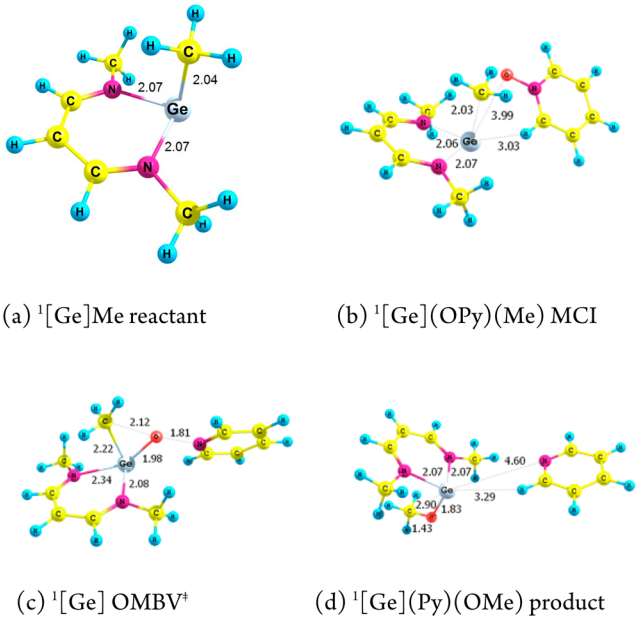

(a) ^{1}[Ge]Me reactant (b) ^{1}[Ge](OPy)(Me) MCI

(c) ^{1}[Ge] OMBV‡ (d) ^{1}[Ge](Py)(OMe) product

Figure 6. Selected B3LYP/CEP-31G(d) optimized geometries of germanium complexes calculated for the OMBV pathway. Bond lengths in Å. The superscript prefix denotes the computed lowest energy multiplicity for that stationary point.

The computed Ge−O bond lengths are 3.99 Å (MCI), 1.98 Å (OMBV‡), and 1.83 Å (product), Figure 6. Thus, the overall decrease in bond length from the OMBV transition state to the methoxide product is δr_{M-O} = 0.15 Å, much more than the 0.02 Å difference computed for the zinc congener and more similar in magnitude to the δr_{M-O} = 0.13 Å calculated for the calcium reaction coordinate.

All germanium complexes are calculated to be singlets in their ground spin states for the preferred oxy-insertion pathway. The triplet multiplicity was considered but was always significantly higher than the singlet. Known divalent germanium compounds—for example germylenes (GeR_2)—are singlets,[35,36]

dx.doi.org/10.1021/ic5015048 | Inorg. Chem. 2014, 53, 7789−7798

which is consistent with the computational prediction of a singlet ground state for [Ge]Me and [Ge]OMe.

We note with interest that an oxo pathway was found for the [Ge]Me + PyO reaction, albeit stationary points for an OAT/MM pathway were always at least 10 kcal/mol *higher* in free energy than corresponding OMBV stationary points. For the OAT/MM pathway, the singlet state was lower than the triplet, with the exception of the methyl migration transition state ($MM^{‡}$), where the triplet TS was 7.8 kcal/mol lower than the corresponding singlet transition state. Basic bonding principles obviously heavily weigh against a formally Ca^{IV}- or Zn^{IV}-oxo, but Ge^{II} does have a filled 4s shell that could conceivably be further oxidized to yield formally Ge^{IV} complexes. Indeed, inspection of the CSD yields seven Ge^{IV}-oxo complexes,[30] suggesting that germanones, although rare in germanium chemistry, are plausible under the right conditions and with the appropriate supporting ligands.

Given the closed-shell electronic configurations of the metal ions computed to operate via a nonredox organometallic-Baeyer–Villiger pathway, Ca^{II} (d^0), Zn^{II} (d^{10}), and Ge^{II}(s^2), it is reasonable to conclude that orbital effects are less important than other considerations such as atomic charge and ionic/covalent radii. An oxy-insertion barrier of >53 kcal/mol for the ^{1}[Ge]Me model is very large and hence unsuitable for both catalytic and stoichiometric purposes. The barrier is approximately double the height computed for oxy-insertion into the metal–carbon bond of [Ca]Me, which displays a more exergonic oxy-insertion, Figure 1. What is perhaps more interesting is that the computed thermodynamics and kinetics for oxy-insertion with ^{1}[Ge]Me, Figure 5, and ^{1}[Zn]Me, Figure 3, are roughly similar. *Taken together, the DFT simulations imply that the main determinant of the OMBV barrier is the exergonicity of the oxy-insertion reaction to form methoxide product.* For a given metal, the [M]–Me + YO → [M]–OMe + Y thermodynamics will be influenced to a great extent by the thermodynamics of the YO/Y couple, i.e., the OAT potential of the oxidant.[46] Given that the methoxide product is in a thermodynamic sink relative to the methyl reactant, *one may posit that identifying systems that oxy-insert at appreciable rates with the weakest (in a thermodynamic sense) oxidants possible is a key design ingredient for MTM catalysis.* Additionally, it may be argued that an important experimental endeavor moving forward is better establishing the linkage between thermodynamic and kinetic OAT potentials for YO/Y couples.

Titanium. All titanium stationary points are computed to be ground state triplets with the exception of the Ti oxygen atom transfer transition state ($OAT^{‡}$) and the Ti^{4+}-oxo-Me intermediate, which are singlets. From separated reactants, the coordination of PyO is exergonic by 22.6 kcal/mol to form the MCI, ^{1}[Ti](OPy)(Me), Figure 7. When starting with the computed geometry of calcium's OMBV transition state, the titanium variant geometry optimized directly toward the OAT/MM pathway for both singlet and triplet states. *Indeed, in the absence of geometric constraints, e.g., of the C–O and N–O bond lengths, an OMBV‡ could not be isolated for the titanium model complex; only those of the OAT/MM variety were found.*

The triplet $OAT^{‡}$ is −7.8 kcal/mol relative to the reactants. For the initial OAT step, the calculated free energy barrier is 14.8 kcal/mol higher than the metallo-Criegee intermediate. The [Ti]–Me pathway thus entails a spin crossover to the singlet surface after the MCI. The triplet state of the oxo-Me intermediate was computed and is much higher, as expected for a d^0 complex, being 48.6 kcal/mol above the singlet oxo.

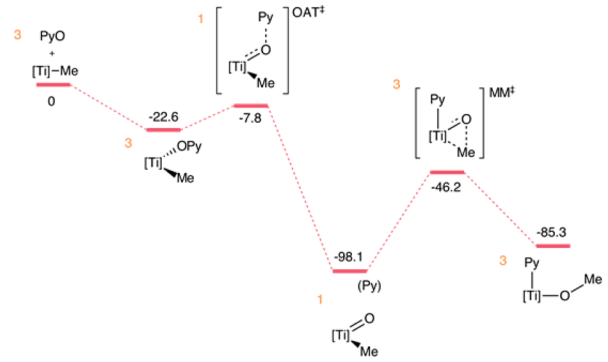

Figure 7. B3LYP/CEP-31G computed reaction coordinate (OAT/MM) for titanium–methyl complex. [Ti] = Ti-β-diketiminate model (see Figure 8). Numerical values are computed free energies in kcal/mol. The superscript prefix denotes the computed lowest energy multiplicity for that stationary point.

The $^3MM^{‡}$ (methyl migration transition state) that connects ^{1}[Ti](O)(Me)·Py to ^{3}[Ti](OMe)·Py is uphill by an enormous 51.9 kcal/mol, Figure 7, and reverts the free energy surface back to the triplet spin state. Even the Ti^{2+}-methoxide product, Figure 8f, is uphill by 12.8 kcal/mol relative to the Ti^{4+}-oxo-Me

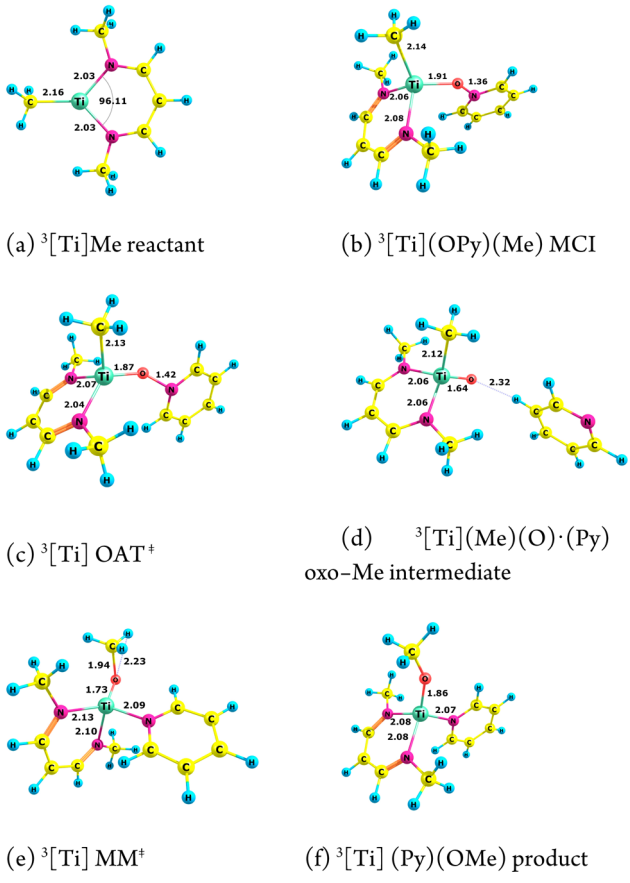

Figure 8. Selected B3LYP/CEP-31G(d) optimized geometries of titanium complexes calculated for the OAT/MM pathway. Bond lengths in Å. The superscript prefix denotes the computed lowest energy multiplicity for that stationary point.

intermediate. It will be seen that titanium is the only metal studied here that proceeds via an OAT mechanism in which the methyl migration transformation is calculated to be endergonic,

dx.doi.org/10.1021/ic5015048 | *Inorg. Chem.* 2014, 53, 7789–7798

likely a reflection of the strong Ti−O π-bond in the formally d^0 oxo intermediate.

Chromium. All chromium complex stationary points are calculated to possess quintet ground states, Figure 9, with the exception of the OAT‡ and [Cr](O)(Me), which are triplets (though the difference between the triplet and the quintet is only 0.8 kcal/mol for the OAT‡, certainly within the error bars of the DFT methods used here). For the oxo-Me intermediate, the singlet state is 25.7 kcal/mol higher than the triplet ground state, and the quintet [Cr](O)(Me)·Py is a further 30.6 kcal/mol higher than the singlet.

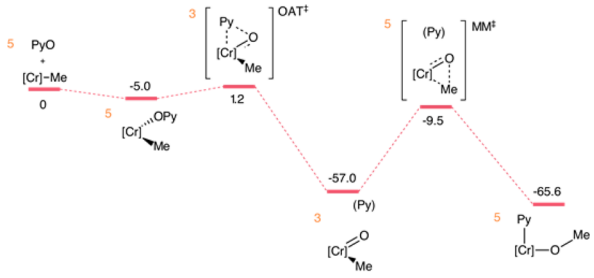

Figure 9. B3LYP/CEP-31G(d) computed reaction coordinate (OAT/MM) for the chromium−methyl complex. [Cr] = Cr-β-diketiminate model (see Figure 10). Numerical values are computed free energies in kcal/mol. The superscript prefix denotes the computed lowest energy multiplicity for that stationary point.

From ^{5}[Cr]Me and pyridine-N-oxide, the reaction coordinate of the chromium complexes is downhill by 5.0 kcal/mol to form the MCI, Figure 9; hence, oxidant binding is less exergonic than the corresponding reaction for the titanium variant, Figure 7. When starting with the computed geometry of calcium's OMBV‡, the chromium analogue (as did the titanium analogue) converged to the OAT/MM pathway for both singlet and triplet states. For the quintet surface, however, an OMBV‡ was found at ΔG_{rel} = 22.2 kcal/mol, and thus the quintet OMBV‡ is 27.2 kcal/mol uphill from the MCI, ^{5}[Cr](OPy)(Me). The singlet OAT‡ is 34.7 kcal/mol higher than the triplet OAT‡. *These computed free energies thus imply that the Cr^{II}−methyl complex would oxy-insert via a two-step, redox pathway mediated by a Cr^{IV}−oxo intermediate in preference to an OMBV pathway.*

The OAT/MM pathway for the chromium complex includes a spin crossover from the quintet MCI to the triplet OAT‡. The quintet OAT‡ is only 0.8 kcal/mol higher in energy than the corresponding triplet transition state, implying facile spin crossover. The oxygen atom transfer barrier is only 6.2 kcal/mol from the MCI (ΔG_{rel} = 1.2 kcal/mol), Figure 9. From the MCI to the triplet Cr^{IV}-oxo-Me intermediate is highly exergonic (ΔG_{rel} = −57.0 kcal/mol). On the way to the MM‡, the chromium triplet oxo-Me intermediate undergoes another spin crossover from the triplet to the quintet surface, engendering a barrier of 47.5 kcal/mol (ΔG_{rel} = −9.5 kcal/mol), Figure 9. At the MM‡ stationary point, Figure 10e, the triplet is calculated to be higher by only 4.6 kcal/mol than the quintet TS, with the singlet 10.4 kcal/mol higher still. Thus, the MM free energy barrier for the chromium MM‡ is only ca. 4 kcal/mol lower than the methyl migration barrier for the Ti analogue, and thus very large, even though the transformation is now mildly exergonic. *As with the titanium case, it is proposed that the large methyl migration barrier reflects the intrinsic strength of the metal−oxygen π bond that must be invested to convert an oxo-methyl complex to the corresponding methoxide for a relatively early transition metal with a low d-electron count.*

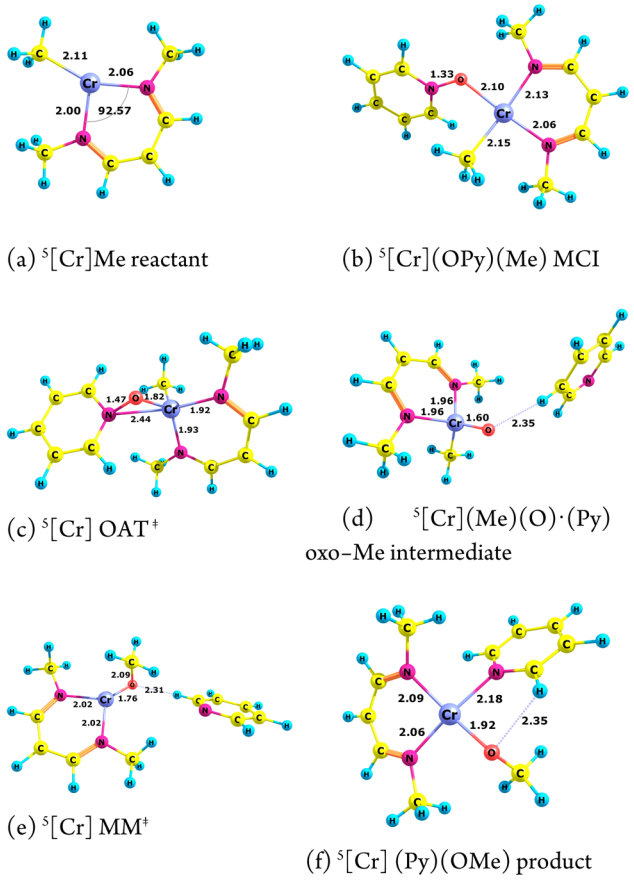

Figure 10. B3LYP/CEP-31G(d) optimized geometries of chromium complexes calculated for the OAT/MM pathway. Bond lengths in Å. The superscript prefix denotes the computed lowest energy multiplicity for that stationary point.

Iron. A quintet was the lowest spin state found for the [Fe]Me reactant, as found experimentally.[41] All stationary points are computed to be quintet ground states. The ^{5}MCI is uphill by only 0.8 kcal/mol versus separated reactants, Figure 11.

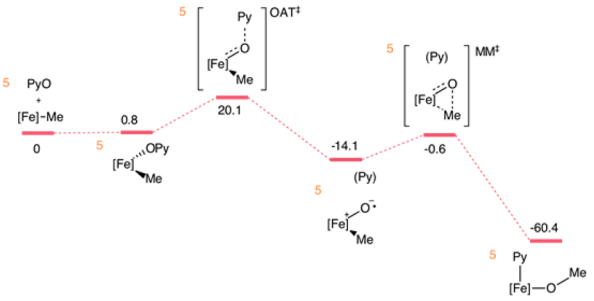

Figure 11. B3LYP/CEP-31G(d) computed reaction coordinate (OAT/MM) for the iron complex. [Fe] = Fe-β-diketiminate model (see Figure 12). Numerical values are computed free energies in kcal/mol. Superscript prefix denotes the computed lowest energy multiplicity for that stationary point.

Though triplet (ΔG_{rel} = 29.6 kcal/mol) and quintet (ΔG_{rel} = 20.1 kcal/mol) OMBV transition states were found, iron was calculated to preferentially oxy-insert via an OAT/MM pathway. From the ^{5}MCI, the ^{5}OAT‡ is 19.3 kcal/mol uphill

dx.doi.org/10.1021/ic5015048 | Inorg. Chem. 2014, 53, 7789−7798

(ΔG_{rel} = 20.1 kcal/mol), and formation of the oxo-Me intermediate is exergonic (ΔG_{rel} = −14.1 kcal/mol). *From the oxo-Me intermediate the methyl migration barrier is only 13.5 kcal/mol,* Figure 11, *much less than for the titanium and chromium congeners.* Given the computed free energy barriers, the initial oxygen atom transfer from PyO to the metal is predicted to be the rate-determining step in the two-step, redox pathway for the model iron−methyl complex.

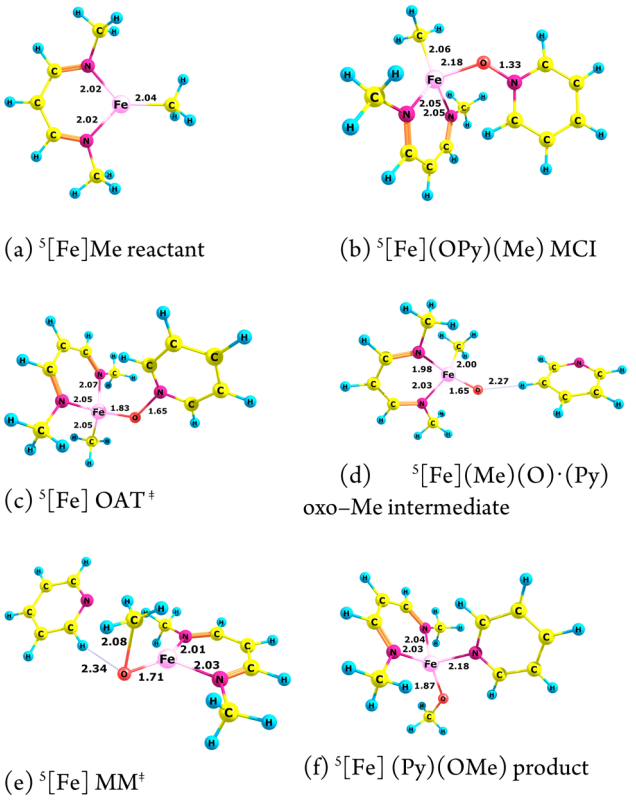

Figure 12. Selected B3LYP/CEP-31G optimized geometries of iron complexes calculated for the OAT/MM pathway. Bond lengths in Å. The superscript prefix denotes the computed lowest energy multiplicity for that stationary point.

One important difference between the iron potential energy surface and the OAT/MM reaction coordinates for the earlier metals is that the Fe-oxo-Me intermediate has increased in free energy relative to the MCI and is no longer in a thermodynamic sink (as is the case with the titanium and chromium complexes, cf. Figures 7, 9, and 11). Occupation of metal dπ−oxo pπ antibonding orbitals has destabilized the formally d^4-Fe^{IV}-oxo-Me intermediate. When compared with the titanium and chromium complexes, the iron analogue has a higher OAT‡ but still remains kinetically accessible with a computed free energy barrier of only 20.1 kcal/mol.

Nickel. All nickel stationary points are computed to be triplet ground states. Binding of PyO to [Ni]Me is uphill by only 2.5 kcal/mol. Though a singlet (ΔG_{rel} = 40.1 kcal/mol) OMBV‡ was found, the lowest energy pathway for nickel goes through the OAT/MM route. From the ^{3}MCI, the ^{3}OAT‡ is 24.1 kcal/mol uphill (ΔG_{rel} = 26.6 kcal/mol). The Ni-oxo-methyl intermediate is mildly endergonic relative to PyO oxidant and the starting methyl complex (ΔG_{rel} = 3.3 kcal/mol). From the triplet oxo-Me intermediate to the corresponding MM‡, a modest 4.0 kcal/mol barrier must be surmounted. As with iron, the methyl migration reaction is calculated to be highly exergonic, Figure 13.

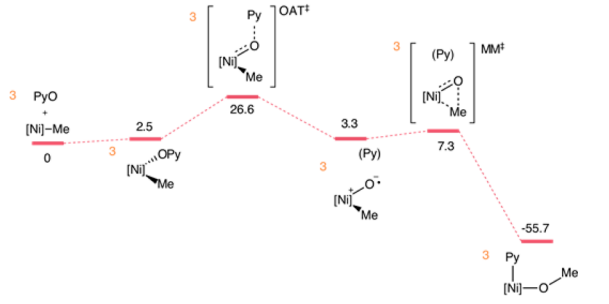

Figure 13. B3LYP/CEP-31G computed reaction coordinate (OAT/MM) for nickel−methyl complex. [Ni] = Ni-β-diketiminate model (see Figure 14). Numerical values are computed free energies in kcal/mol. The superscript prefix denotes the computed lowest energy multiplicity for that stationary point.

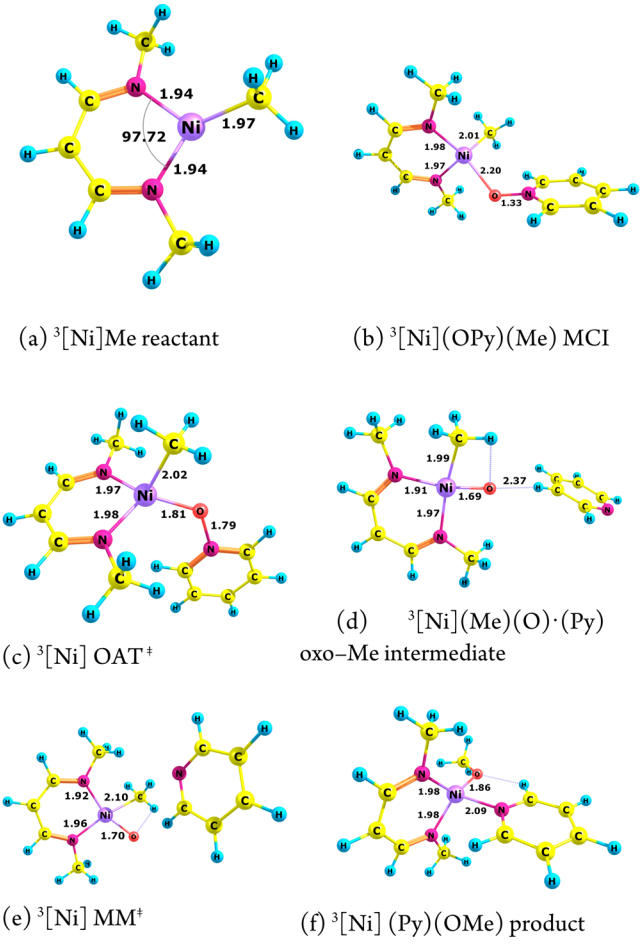

Figure 14. Selected B3LYP/CEP-31G(d) optimized geometries of nickel complexes calculated for the OAT/MM pathway. Bond lengths in Å. The superscript prefix denotes the computed lowest energy multiplicity for that stationary point.

SUMMARY, CONCLUSIONS, AND PROSPECTUS

Several important conclusions have emerged from the present modeling study of oxy-insertion into metal−methyl bonds by both redox and nonredox processes for a series of seven β-diketiminate-methyl complexes spanning the 3d series from

dx.doi.org/10.1021/ic5015048 | Inorg. Chem. 2014, 53, 7789−7798

the s-block (Ca) to the p-block (Ge). The most important among these are summarized here.

(1) The nonredox OMBV pathway was computed to be preferred for two non-d^0 metals: the d^{10} Zn^{II}–methyl complex and the post-transition metal Ge^{II}–methyl complex. Although these are non-d^0 complexes, simulations suggest that *the organometallic Baeyer–Villiger mechanism for oxy-insertion is preferred only in those cases when the d^n electron count is such that a formal two electron oxidation of [M]–Me reactant to yield a oxo-methyl intermediate would render a chemically infeasible formal oxidation state*, e.g., Zn^{IV}-oxo. Even for the Ge^{II}–methyl model, the OMBV pathway, which requires oxidation of the $4s^2$ subshell, is found to be not much further lower in energy than the competing redox ($Ge^{II} \Leftrightarrow Ge^{IV}$) pathway.

(2) From a catalytic standpoint, one would like to "flatten" the reaction coordinate for oxy-insertion. The results for iron and nickel suggest that increasing d^n ($n > 2$) will destabilize $L_nM(O)(Me)$ intermediates. Hence, *by moving closer to the oxo wall,*[20,31,32] *the first thermodynamic sink (oxo-Me intermediate) in the OAT/MM pathway is removed.* However, with appropriate metals and ligands, such entities remain kinetically accessible; see Figure 15 for the iron (purple) and nickel (cyan) reaction coordinates. Additionally, methyl migration—which has emerged as a difficult transformation in organic[16] and organometallic[47] Baeyer–Villiger oxidations—is facile with barriers less than 14 kcal/mol for both iron and nickel β-diketiminate models.

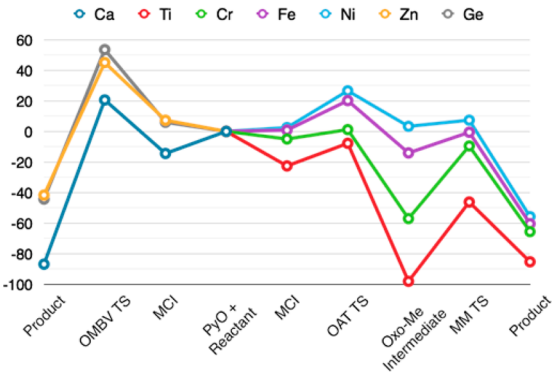

Figure 15. B3LYP/CEP-31G(d) computed reaction coordinate for $[M^{II}]$–Me + PyO → $[M^{II}]$–OMe + Py for M = {Ca, Ti, Cr, Fe, Ni, Zn, Ge}. Numerical values are computed free energies (kcal/mol). Metals computed to operate via an OMBV (oxo-mediated) mechanism are to the left (right) of the reactants. Separated "PyO + [M]Me" reactants define the zero free energy point. OMBV TS = organometallic Baeyer–Villiger (nonredox) TS; product = [M]–OMe + Py; OAT TS = oxygen atom transfer transition state; Oxo-Me = oxo-methyl intermediate, [M](O)(Me)·Py; MM TS = methyl migration transition state; MCI (metallo-Criegee intermediate) or [M](Me)(PyO) adduct.

Table 1 lists the spin densities on the metal and oxygen atoms for open-shell oxo-methyl intermediates ([Ti](Me)(O) is a singlet). Both the iron and nickel species have substantial spin density on the oxygen ligand. The present results, in conjunction with previous contributions from our group,[14] thus identify two factors in facilitating methyl migration to form the C–O bond needed for hydrocarbon functionalization. First, there must be a reduction in the strength of the metal–oxygen π-bond that is sacrificed as the methyl-oxo transforms into a methoxide ligand. Second, reduction in nucleophilicity of the oxygen ligand as it transforms more from an early transition metal oxide (O^{2-}) to more of an oxyl ($O^{\bullet -}$) description for midlater series transition metals is also important.

Table 1. Atomic Spin Densities (e^-) from a Mulliken Population Analysis of the Lowest Energy oxo-Me Intermediates for Open-Shell Species[a]

M	ρ_{spin}(M)	ρ_{spin}(O)
Ti	singlet	
^{3}Cr	2.3	0.2
^{5}Fe	3.4	0.6
^{3}Ni	0.8	1.1

[a]Multiplicity of the oxo-Me intermediate is indicated by the superscript numeral.

(3) There seems to be no inherent kinetic or thermodynamic advantage between the OMBV and OAT/MM pathways, Figure 15. Kinetically, the most feasible [M]Me show computed oxy-insertion free energy barriers of ~20 kcal/mol for the rate-determining step for either mechanism with pyridine-N-oxide as the oxidant. In the present research *for all transition metals predicted to operate via a two-step OAT/MM pathway, the transition state leading to $L_nM(O)(R)$ was computed to be the highest point on the* reaction *coordinate for oxy-insertion.* The main challenge for d^0 complexes that operate via OMBV pathways is that such species seem incapable of activating strong, aliphatic C–H bonds unless they are three-coordinate.[48−50] Thermodynamically, *both oxy-insertion mechanisms suffer from the same feature that would thwart MTM catalysis, i.e., the $[M^{II}]$-methoxide product is in a thermodynamic sink relative to the $[M^{II}]$-methyl reactant* with computed exergonicities of 40 kcal/mol or more for the reaction.

(4) The latter point raises a critical question moving forward in methane-to-methanol catalysis: how may one destabilize the L_nM–OMe product while not making the barriers leading to it too high? Consider the overall oxy-insertion reaction, eq 1.

$$L_nM\text{–Me} + YO \rightarrow L_nM\text{–OMe} + Y \quad (1)$$

Large exergonicities for oxy-insertion, eq 1, are computed for all metals studied herein, regardless of d-orbital occupation, mechanism of oxy-insertion, location within the periodic table, and hence the relative covalent/ionic radii, oxophilicity, and electronegativity of the metal etc. As such, it is evident that the strength of the oxidant/leaving group (YO/Y) couple is important in eq 1. What is perhaps paradoxical is the implication from the present computations that *future experiments in hydrocarbon partial oxidation catalysis should focus on effecting the oxy-insertion transformations with the weakest oxidants* (in a thermodynamic sense) given the large thermodynamic driving forces computed for oxy-insertion. Perhaps what is more germane in terms of rational design of organometallic complexes to perform selective oxy-insertion is a better understanding of the correlation between thermodynamic and kinetic OAT potentials. The former are abundant thanks to the classic review by Holm and Donahue,[46] as well as updates by Holm and Lee.[51] There is little pertinent information in regards to the correlation between thermodynamic and kinetic OAT potentials, which would seem to be an area in which computational chemistry could greatly assist the hunt for new catalysts.

Figure 15 makes it obvious that the most encouraging systems are Fe and Ni, the issue of methoxide product stability notwithstanding. The OAT and MM barriers are both reasonable, and while the oxo-Me intermediates are destabilized relative to earlier, lower d-count metals, the DFT computations

dx.doi.org/10.1021/ic5015048 | Inorg. Chem. 2014, 53, 7789–7798

suggest they are still thermodynamically and kinetically accessible. For iron, the OAT free energy barrier is 20 kcal/mol while for the nickel variant it is 27 kcal/mol. Assuming $\Delta G^{\ddagger} <$ 30 kcal/mol as a target for a low-temperature MTM process, then there is more room for maneuvering in the Fe^{II} case than the Ni^{II} model. Given the more or less methodical transformation of the curves in Figure 15 with d-count, one may also infer that the intervening Co^{II}–methyl complexes are worthy of experimental and computational scrutiny. Preliminary simulations of oxy-insertion reactions of [Co]Me and [Mn]Me with PyO indicate that they follow the trends displayed by the even d-count that flank them.

Simulations suggest that it is desirable to destabilize [M]–OMe relative to [M]–Me if the ultimate goal is efficient catalysis. In this regard, the [Ni]–Me/–OMe couple is only slightly less exergonic than the iron complex, $\Delta G_{rxn} = -56$ (Fe), −60 (Ni) kcal/mol. Moving closer to the oxo wall was computed to remove the oxo-Me intermediate from its thermodynamic "sink," but of course, both [M]–OMe and [M]–Me have the same formal oxidation state. Sterics would seem to be a less profitable strategy to influence the thermodynamics of oxy-insertion since both the ultimate reactant [M]–Me and product [Me]–OMe are the same coordination number (assuming the leaving group Y does indeed leave) and the OMe substituent of the product should be smaller than the Me substituent of the reactant (cf. a cone angle[52] of $PMe_3 \sim 120°$ and $\sim 110°$ for $P(OMe)_3$). Thus, the intrinsic thermodynamic favorability of oxy-insertion could be ameliorated through a judicious choice of supporting ligand (a) trans influence/effect (methyl is a very strong trans influence/effect ligand while methoxide is less) and/or (b) acid/base properties (methide is a stronger base than methoxide), which thus also define profitable research endeavors.

■ ASSOCIATED CONTENT

Ⓢ Supporting Information

Cartesian coordinates and computed free energies of all calculated species and full citations for ref 21. This material is available free of charge via the Internet at http://pubs.acs.org.

■ AUTHOR INFORMATION

Corresponding Author

*E-mail: t@unt.edu.

Notes

The authors declare no competing financial interest.

■ ACKNOWLEDGMENTS

This work was solely supported as part of the Center for Catalytic Hydrocarbon Functionalization, an Energy Frontier Research Center funded by the U.S. Department of Energy, Office of Science, Office of Basic Energy Sciences under Award Number DE-SC0001298.

■ REFERENCES

(1) Olah, G. A. *Angew. Chem., Int. Ed.* **2005**, *44*, 2636–2639.
(2) Timmermans, P.; Van Haute, A. *Water Res.* **1983**, *17*, 1249–1255.
(3) Wagner, M.; Loy, A.; Nogueira, R.; Purkhold, U.; Lee, N.; Daims, H. *Antonie van Leeuwenhoek* **2002**, *81*, 665–680.
(4) Olah, G. A.; Molnár, A. r. d. *Hydrocarbon Chemistry*, 2nd ed.; Wiley-Interscience: Hoboken, NJ, 2003; p xxiv, 871.
(5) Labinger, J. A. *J. Mol. Catal. A: Chem.* **2004**, *220*, 27–35.
(6) Periana, R. A.; Bhalla, G.; Tenn Iii, W. J.; Young, K. J. H.; Liu, X. Y.; Mironov, O.; Jones, C. J.; Ziatdinov, V. R. *J. Mol. Catal. A: Chem.* **2004**, *220*, 7–25.
(7) Goldman, A. S.; Goldberg, K. I. *ACS Symp. Series* **2004**, *885*, 1–43.
(8) Stahl, S. S.; Labinger, J. A.; Bercaw, J. E. *Angew. Chem., Int. Ed.* **1998**, *37*, 2180–2192.
(9) Arndtsen, B. A.; Bergman, R. G. *Science* **1995**, *270*, 1970–1973.
(10) Janowicz, A. H.; Bergman, R. G. *J. Am. Chem. Soc.* **1983**, *105*, 3929–3939.
(11) Burger, P.; Bergman, R. G. *J. Am. Chem. Soc.* **1993**, *115*, 10462–10463.
(12) Shilov, A. E.; Shul'pin, G. B. *Chem. Rev.* **1997**, *97*, 2879–2932.
(13) Figg, T. M.; Cundari, T. R.; Gunnoe, T. B. *Organometallics* **2011**, *30*, 3779–3785.
(14) Figg, T. M.; Cundari, T. R. *Organometallics* **2012**, *31*, 4998–5004.
(15) Pouy, M. J.; Milczek, E. M.; Figg, T. M.; Otten, B. M.; Prince, B. M.; Gunnoe, T. B.; Cundari, T. R.; Groves, J. T. *J. Am. Chem. Soc.* **2012**, *134*, 12920–12923.
(16) Renz, M.; Meunier, B. *Eur. J. Org. Chem.* **1999**, *1999*, 737–750.
(17) Vesborg, P. C. K.; Jaramillo, T. F. *RSC Adv.* **2012**, *2*, 7933–7947.
(18) Mei, J.; Carsch, K. M.; Freitag, C. R.; Gunnoe, T. B.; Cundari, T. R. *J. Am. Chem. Soc.* **2012**, *135*, 424–435.
(19) Bischof, S. M.; Cheng, M.-J.; Nielsen, R. J.; Gunnoe, T. B.; Goddard, W. A.; Periana, R. A. *Organometallics* **2011**, *30*, 2079–2082.
(20) Van Asselt, A.; Trimmer, M. S.; Henling, L. M.; Bercaw, J. E. *J. Am. Chem. Soc.* **1988**, *110*, 8254–8255.
(21) Frisch, M. J.; Trucks, G. W.; Schlegel, H. B.; Scuseria, G. E.; Robb, M. A.; Cheeseman, J. R.; Scalmani, G.; Barone, V.; Mennucci, B.; Petersson, G. A.; Nakatsuji, H.; Caricato, M.; Li, X.; Hratchian, H. P.; Izmaylov, A. F.; Bloino, J.; Zheng, G.; Sonnenberg, J. L.; Hada, M.; Ehara, M.; Toyota, K.; Fukuda, R.; Hasegawa, J.; Ishida, M.; Nakajima, T.; Honda, Y.; Kitao, O.; Nakai, H.; Vreven, T.; Montgomery, J. A.; Peralta, J. E.; Ogliaro, F.; Bearpark, M.; Heyd, J. J.; Brothers, E.; Kudin, K. N.; Staroverov, V. N.; Kobayashi, R.; Normand, J.; Raghavachari, K.; Rendell, A.; Burant, J. C.; Iyengar, S. S.; Tomasi, J.; Cossi, M.; Rega, N.; Millam, J. M.; Klene, M.; Knox, J. E.; Cross, J. B.; Bakken, V.; Adamo, C.; Jaramillo, J.; Gomperts, R.; Stratmann, R. E.; Yazyev, O.; Austin, A. J.; Cammi, R.; Pomelli, C.; Ochterski, J. W.; Martin, R. L.; Morokuma, K.; Zakrzewski, V. G.; Voth, G. A.; Salvador, P.; Dannenberg, J. J.; Dapprich, S.; Daniels, A. D.; Farkas; Foresman, J. B.; Ortiz, J. V.; Cioslowski, J.; Fox, D. J. *Gaussian 09*, revision C.01; Gaussian, Inc.: Wallingford, CT, 2009.
(22) Vosko, S. H.; Wilk, L.; Nusair, M. *Can. J. Phys.* **1980**, *58*, 1200–1211.
(23) Becke, A. D. *J. Chem. Phys.* **1993**, *98*, 5648–52.
(24) Lee, C.; Yang, W.; Parr, R. G. *Phys. Rev. B* **1988**, *37*, 785–789.
(25) Stephens, P. J.; Devlin, F. J.; Chabalowski, C. F.; Frisch, M. J. *J. Phys. Chem.* **1994**, *98*, 11623–11627.
(26) Stevens, W. J.; Krauss, M.; Basch, H.; Jasien, P. G. *Can. J. Chem.* **1992**, *70*, 612–630.
(27) Poli, R.; Harvey, J. N. *Chem. Soc. Rev.* **2003**, *32*, 1–8.
(28) Harvey, J.; Aschi, M. *Phys. Chem. Chem. Phys.* **1999**, *1*, 5555–5563.
(29) Harvey, J. N.; Aschi, M.; Schwarz, H.; Koch, W. *Theor. Chem. Acc.* **1998**, *99*, 95–99.
(30) Allen, F. H. *Acta Crystallogr., Sect. B: Struct. Sci.* **2002**, *58*, 380–8.
(31) Ballhausen, C. J.; Gray, H. B. *Molecular Orbital Theory; an Introductory Lecture Note and Reprint Volume*; Ballhausen, C. J., Gray, H. B., Eds.; W.A. Benjamin: New York, 1964; p ix, 273.
(32) Ballhausen, C. J.; Gray, H. B. *Molecular Electronic Structures: an Introduction*; Benjamin/Cummings Pub. Co.: Reading, MA, 1980; Advanced Book Program, p viii, 138.
(33) Ballhausen, C. J.; Gray, H. B. *Inorg. Chem.* **1962**, *1*, 111–122.

(34) Prust, J.; Stasch, A.; Zheng, W.; Roesky, H. W.; Alexopoulos, E.; Usón, I.; Böhler, D.; Schuchardt, T. *Organometallics* **2001**, *20*, 3825−3828.
(35) Saur, I.; Miqueu, K.; Rima, G.; Barrau, J.; Lemierre, V.; Chrostowska, A.; Sotiropoulos, J.-M.; Pfister-Guillouzo, G. *Organometallics* **2003**, *22*, 3143−3149.
(36) Ding, Y.; Ma, Q.; Roesky, H. W.; Herbst-Irmer, R.; Usón, I.; Noltemeyer, M.; Schmidt, H.-G. *Organometallics* **2002**, *21*, 5216−5220.
(37) Fan, H.; Adhikari, D.; Saleh, A. A.; Clark, R. L.; Zuno-Cruz, F. J.; Sanchez Cabrera, G.; Huffman, J. C.; Pink, M.; Mindiola, D. J.; Baik, M.-H. *J. Am. Chem. Soc.* **2008**, *130*, 17351−17361.
(38) Nikiforov, G. B.; Roesky, H. W.; Heisen, B. C.; Grosse, C.; Oswald, R. B. *Organometallics* **2008**, *27*, 2544−2548.
(39) Zhao, G.; Basuli, F.; Kilgore, U. J.; Fan, H.; Aneetha, H.; Huffman, J. C.; Wu, G.; Mindiola, D. J. *J. Am. Chem. Soc.* **2006**, *128*, 13575−13585.
(40) Kilgore, U. J.; Basuli, F.; Huffman, J. C.; Mindiola, D. J. *Inorg. Chem.* **2005**, *45*, 487−489.
(41) Holland, P. L.; Cundari, T. R.; Perez, L. L.; Eckert, N. A.; Lachicotte, R. J. *J. Am. Chem. Soc.* **2002**, *124*, 14416−14424.
(42) Figg, T. M.; Webb, J. R.; Cundari, T. R.; Gunnoe, T. B. *J. Am. Chem. Soc.* **2012**, *134*, 2332−2339.
(43) Ess, D. H.; Gunnoe, T. B.; Cundari, T. R.; Goddard, W. A.; Periana, R. A. *Organometallics* **2010**, *29*, 6801−6815.
(44) Biyikal, M.; Löhnwitz, K.; Meyer, N.; Dochnahl, M.; Roesky, P. W.; Blechert, S. *Eur. J. Inorg. Chem.* **2010**, *2010*, 1070−1081.
(45) Shannon, R. *Acta Crystallogr., Sect. A* **1976**, *32*, 751−767.
(46) Holm, R. H.; Donahue, J. P. *Polyhedron* **1993**, *12*, 571−589.
(47) Conley, B. L.; Ganesh, S. K.; Gonzales, J. M.; Tenn, W. J., III; Young, K. J. H.; Oxgaard, J.; Goddard, W. A., III; Periana, R. A. *J. Am. Chem. Soc.* **2006**, *128*, 9018−9019.
(48) Bennett, J. L.; Wolczanski, P. T. *J. Am. Chem. Soc.* **1994**, *116*, 2179−2180.
(49) Cummins, C. C.; Baxter, S. M.; Wolczanski, P. T. *J. Am. Chem. Soc.* **1988**, *110*, 8731−8733.
(50) Schaller, C. P.; Wolczanski, P. T. *Inorg. Chem.* **1993**, *32*, 131−144.
(51) Lee, S. C.; Holm, R. H. *Inorg. Chim. Acta* **2008**, *361*, 1166−1176.
(52) Tolman, C. A. *J. Am. Chem. Soc.* **1970**, *92*, 2956−2965.